SF2A 2009
M. Heydari-Malayeri, C. Reylé and R. Samadi (eds)

COSMOLOGICAL SIMULATIONS AND GRAVITATIONAL LENSING: STATISTICAL SIGNATURES OF SUBSTRUCTURES

Peirani, S.[1], Alard, C.[1], Pichon, C.[1], Gavazzi, R.[1] and Aubert, D.[2]

Abstract. The popular model of hierarchical structure formation in a universe dominated by cold dark matter, while quite successful in matching the observed large-scale density distribution, is currently facing a "small-scale crisis". For instance, the predicted abundance of satellites (or substructures) is more than an order of magnitude larger than the number of dwarf galaxies with comparable mass within the local group. This "missing satellite problem" represents then an ideal framework in order to test theoretical models. We present a new approach, based on numerical modelling and a perturbative theory, to study and characterize statistical signatures of substructures in the strong lensing regime.

1 Introduction

The cold dark matter (CDM) paradigm (Cole et al. 2005 and references therein) has led to a successful explanation of the large-scale structure in the galaxy distribution on scales $0.02 \leq k \leq 0.15$h Mpc^{-1}. In spite of these impressive successes, there are still discrepancies between simulations and observations on scales ≤ 1 Mpc, extensively discussed in the recent literature. For instance, one problem that requires closer examination concerns the large number of sub-L_* subhalos present in simulations but not observed (Kauffmann, White & Guiderdoni 1993; Moore et al. 1999; Klypin et al. 1999).

This "missing satellite problem" remains an ideal framework to test cosmological models. During the past years, different methods have been employed in order to study the gravitational potential of groups or clusters of galaxies, for instance through their X-ray lines emission of hot gas in the intra-cluster medium or through lensing considerations. However, while lensing directly probes the mass distribution in those objects, the other methods rely more often than not on strong hypotheses on the dynamical state of the gas and interactions between baryons and dark matter. For example, the gas is supposed to be in hydrostatical equilibrium in the gravitational potential well created by dark matter halo, while spherical symmetry is assumed.

In Peirani et al. (2008), we have studied the effects induced by substructures on the deflection potential of dark matter halos in the strong lensing regime. The presence of substructures follows from the capture of small satellites which have not yet been disrupted by tidal forces and/or suggests that the relaxation of halos is not totally finished. One interesting alternative approach is to treat all deviations from a circularly symmetrical potential as small perturbations (Alard 2007, 2008) defining the location where multiple extended images will form (see Fig. 1).

This paper is organized as follows: section 2 first sketches the pertubative lens solution while section 3 presents our main results on the statistics of perturbations.

2 A perturbative theory

The general lens equation, relating the position of an image on the lens plane to that of the source on the source plane can be written in polar coordinates as

$$\mathbf{r_s} = \Big(r - \frac{\partial \phi}{\partial r}\Big)\mathbf{u_r} - \Big(\frac{1}{r}\frac{\partial \phi}{\partial \theta}\Big)\mathbf{u}_\theta \,, \tag{2.1}$$

[1] Institut d'Astrophysique de Paris, 98 bis Bd Arago, 75014 Paris, France -
Unité mixte de recherche 7095 CNRS - Université Pierre et Marie Curie.
[2] Observatoire Astronomique de Strasbourg, 11 Rue de l'Université, 67000 Strasbourg, France.

where $\mathbf{r}_s$ is the source position, and r, $\mathbf{u}_r$ and $\mathbf{u}_\theta$ are the radial distance, radial direction and orthoradial direction respectively. Here $\phi(r,\theta)$ is the projected potential. The basics ideas of the perturbative approach is to expand equation (2.1) by introducing i) small displacements of the source from the origin and ii) non-circular perturbation of the potential, ψ which can be described by:

$$r_s = \epsilon r_s\,, \quad \text{and} \quad \phi = \phi_0 + \epsilon\psi\,, \tag{2.2}$$

where ϵ is small number: $\epsilon \ll 1$. To obtain image positions (r,θ) by solving equation (2.1) directly, may prove to be analyically impossible in the general case. It is then easier to find perturbative solution by inserting equation (2.2) into equation (2.1). And using the Taylor expansion of ϕ:

$$\phi = \phi_0 + \epsilon\psi = \sum_{n=0}^{\infty}[C_n + \epsilon f_n(\theta)](r-1)^n \quad where \quad C_n \equiv \frac{1}{n!}\Big[\frac{d^n\phi_0}{dr^n}\Big]_{r=1} \; and \quad f_n(\theta) \equiv \frac{1}{n!}\Big[\frac{\partial^n\psi}{\partial r^n}\Big]_{r=1}, \tag{2.3}$$

one can finally obtain the general perturbative response (Alard 2007):

$$\mathbf{r_s} = (\kappa_2\delta r - f_1)\mathbf{u}_r - \frac{\mathrm{d}f_0}{\mathrm{d}\theta}\mathbf{u}_\theta \quad with \quad \kappa_2 = 1 - 2C_2. \tag{2.4}$$

In the perturbative theory, all deviations from the perfect ring configuration is in two fields, f_1 and $\frac{\mathrm{d}f_0}{\mathrm{d}\theta}$: f_1 gives informations of the mean position of the contour lines whereas $\frac{\mathrm{d}f_0}{\mathrm{d}\theta}$ gives informations about the image width along the radial direction (see Fig 2).

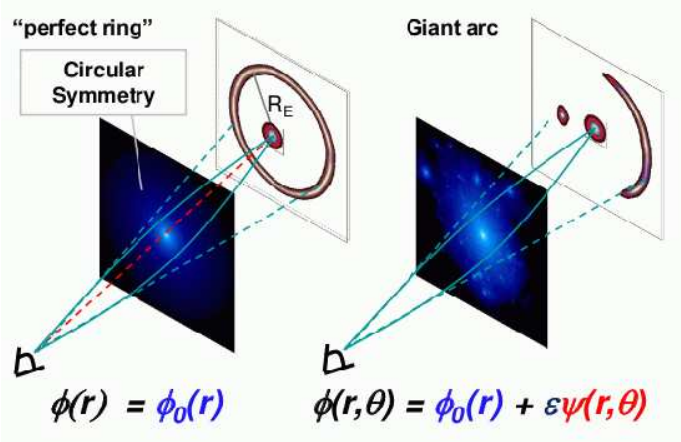

Fig. 1. Sketch about the Einstein ring (left part) and the giant arc (right part) configurations.

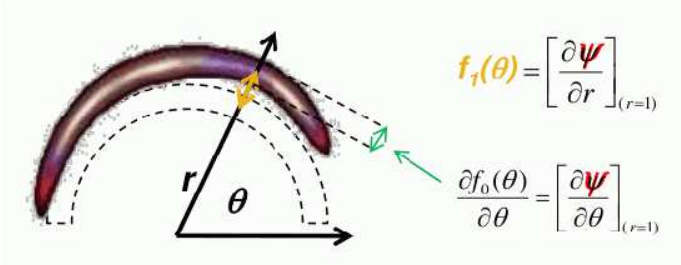

Fig. 2. Sketch about the interpretation of f_1 and $\frac{\mathrm{d}f_0}{\mathrm{d}\theta}$ in term of deviations from the perfect ring.

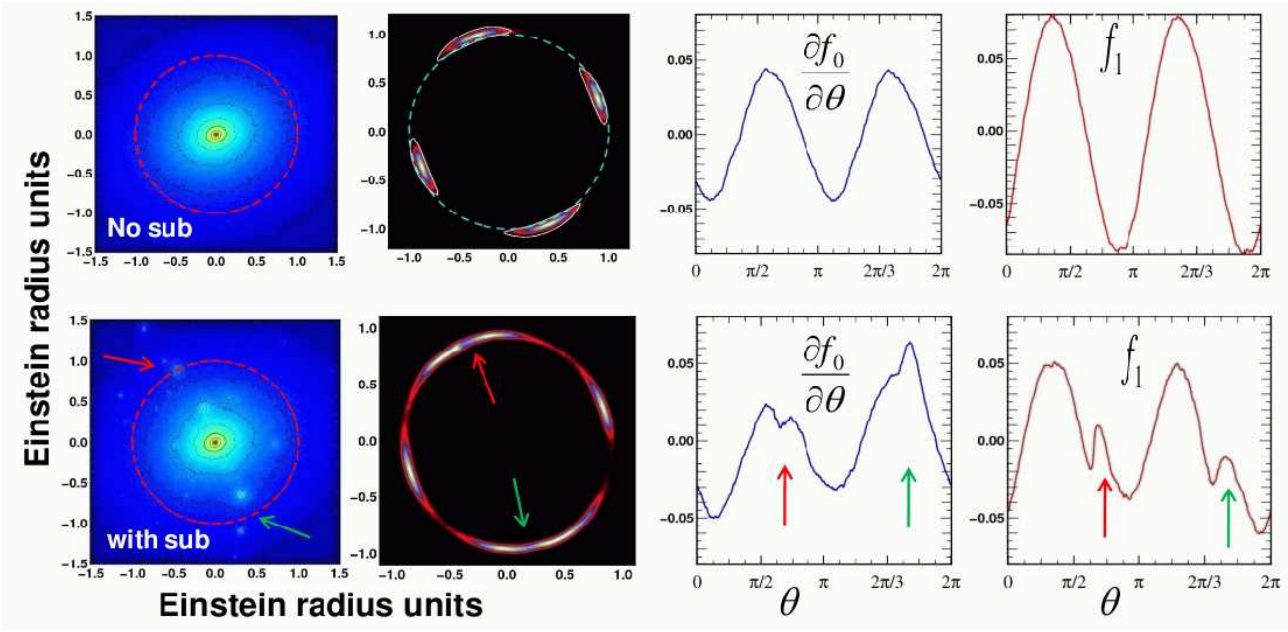

Fig. 3. Projected density map of a lens modelled by a dark matter halo with and without substructures. The respective solutions from ray-tracing simulations are plotted in the second column. Finally, columns 3 and 4 show the evolution of f_1 and $\frac{\mathrm{d}f_0}{\mathrm{d}\theta}$ for each associated lens.

3 Numerical modelling and statistical effects of substructures

Lenses are modelled either by dark matter halos extracted from cosmological simulations or via toy models. The advantage of toy models is to reach a higher resolution and to allow us to study the influence of free parameters such as the inner profiles of substructures which are expected to play a central role here. For instance, the sample A represents our reference catalogue in which all halos have no substructure. For each of them, we introduce a fraction of subtructures. These halos are classified in catalogues B and C according the definition of inner density profile of clumps. For example, each halo from samples B1 and B2 have 15% of substructures with an inner profile represented by a cusp whereas lenses catalogues C1 and C2 have substructures represented by a core profile with $C_{sub} = 5$ and $C_{sub} = 8$ respectively.

In Figure (3), we show the projected mass density of the same lens with and without substructures near the Einstein radius, the image's solution obtained from ray-tracing (when an elliptical source is placed at the origin) and the evolutions of f_1 and $\frac{\mathrm{d}f_0}{\mathrm{d}\theta}$. As expected, when no substructure are considered, we obtain four distinct arcs in a cross configuration. From a theoretical point of view, it is easy to show that the functions $f_1$and $\frac{\mathrm{d}f_0}{\mathrm{d}\theta}$are proportional to $\propto \cos(2\theta + \psi)$ and $\propto \sin(2\theta + \psi)$ respectively. These functionnal form are recovered in our experiment and shown in Figure (3).

When substructures are present, the shape of images is significantly altered. First, we notice that the positions of substructure tend to break the ellipticity of the halo center. Thus, it is not surprising that the shape of the image is approaching a ring in that case. Moreover, it is interesting to see that the position of one substructure (at the top left of the figure) is exactly at the Einstein radius. This produces an alteration of the luminosity. This effect can be clearly seen when comparing the perturbative fields $f_1$and $\frac{\mathrm{d}f_0}{\mathrm{d}\theta}$relative to the lens L_1 in Figure (3). For instance, we can see two clear bumps in the evolution of $\frac{\mathrm{d}f_0}{\mathrm{d}\theta}$. The second one ($\theta > 2\pi/3$) is produced by substructures in the lower right part and induced an alteration of the luminosity again.

The angular functions $f_1$and $\frac{\mathrm{d}f_0}{\mathrm{d}\theta}$can be characterized by their Fourier expansion:

$$\frac{df_0(\theta)}{\mathrm{d}\theta} = \sum_n \langle a_n^0 \rangle \cos\left(n\theta + \phi_n^0\right) , \tag{3.1}$$

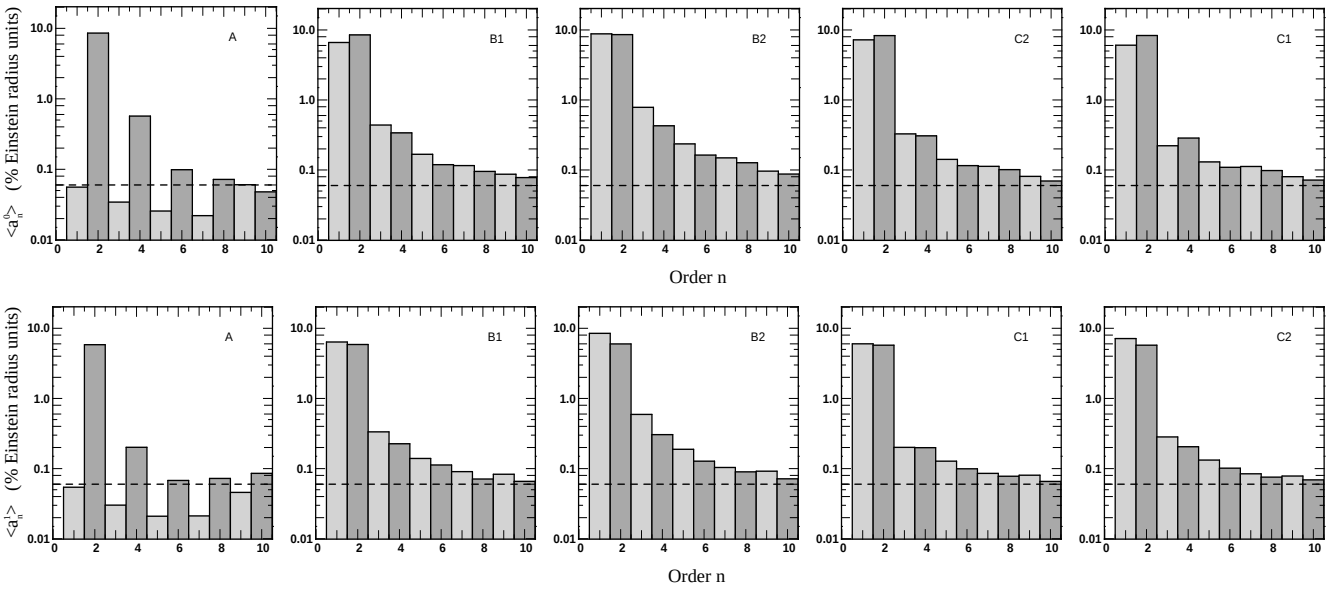

Fig. 4. Variation of mean amplitudes $\langle a_n^0 \rangle$ (first line) and $\langle a_n^1 \rangle$ (second line) derived from multipole expansions of $\frac{\mathrm{d}f_0}{\mathrm{d}\theta}$ and f_1 respectively for lenses catalogue A, B_1, B_2, C_1 et C_2. The dashed lines represent limits at 1σ.

$$f_1(\theta) \quad = \quad \sum_n \langle a_n^1 \rangle \cos\left(n\theta + \phi_n^1\right) \, , \tag{3.2}$$

where $P_i(n)$, $i = 1, 2$ correspond to associated power spectra. We have derived the multipole expansion of $f_1$and $\frac{\mathrm{d}f_0}{\mathrm{d}\theta}$for each halo of the different catalogues and we focus in the following on the mean amplitudes $\langle a_n^0 \rangle$ and $\langle a_n^1 \rangle$ obtained (see Fig. 4). When substructures are absent, both harmonic power spectra of $f_1$and $\frac{\mathrm{d}f_0}{\mathrm{d}\theta}$are dominated by the second order mode, which is characteristic of a projected elliptical potential. The situation is totally different when substructures are taken into account. First, we notice that first mode ($n = 1$) increase for lenses L_1 and L_2. This is due to the fact that we kept the same definition of the mass center between the three lenses. The random position of subtructures generates a non zero impact parameter which affect the first order mode. Moreover, since substructures tend to break the ellipticity of the halo center in the present case, one expects that the second mode decreases. However, the most interesting feature is that modes corresponding to $n \geq 3$ increase when substructures are present.

4 Conclusions and perspectives

The upcoming generation of high spatial resolution instruments dedicated to cosmology (*e.g.* JWST, DUNE, SNAP, ALMA) will provide us with an unprecedented number of giant arcs at all scales. The large samples expected will make standard lens modellings untractable and require the development of new methods able to capture the most relevant source of constraints for cosmology. In this respect, the perturbative method we present here may turn out to be a promising research line.

References

Alard, C. 2007, MNRAS, 382, L58
Alard, C. 2008, MNRAS, 388, 375
Cole, S., et al. 2005, MNRAS, 362, 505
Kauffmann G., White S. D. M. & Guiderdoni B., 1993, MNRAS 264, 201
Klypin A., Kravtsov A. V., Valenzuela O. & Prada F., 1999, ApJ 522, 82
Moore B., Ghigna S., Governato F., Lake G., Quinn T., Stadel J. & Tozzi P., 1999, ApJ 524, L19
Peirani, S., Alard, C., Pichon, C., Gavazzi, R., & Aubert, D. 2008, MNRAS, 390, 945